nature biomedical engineering

ARTICLES

https://doi.org/10.1038/s41551-020-00607-7

Check for updates

The sustained expression of Cas9 targeting toxic RNAs reverses disease phenotypes in mouse models of myotonic dystrophy type 1

Ranjan Batra[1,2,3,4,8], David A. Nelles[1,2,3,4,8], Daniela M. Roth[4], Florian Krach[1,2,3], Curtis A. Nutter[5], Takahiro Tadokoro[6], James D. Thomas[5], Łukasz J. Sznajder[5], Steven M. Blue[1,2,3], Haydee L. Gutierrez[4], Patrick Liu[4], Stefan Aigner[1,2,3], Oleksandr Platoshyn[7], Atsushi Miyanohara[7], Martin Marsala[7], Maurice S. Swanson[5] and Gene W. Yeo[1,2,3] ✉

Myotonic dystrophy type I (DM1) is a multisystemic autosomal-dominant inherited human disorder that is caused by CTG microsatellite repeat expansions (MREs) in the 3′ untranslated region of *DMPK*. Toxic RNAs expressed from such repetitive sequences can be eliminated using CRISPR-mediated RNA targeting, yet evidence of its in vivo efficacy and durability is lacking. Here, using adult and neonatal mouse models of DM1, we show that intramuscular or systemic injections of adeno-associated virus (AAV) vectors encoding nuclease-dead Cas9 and a single-guide RNA targeting CUG repeats results in the expression of the RNA-targeting Cas9 for up to three months, redistribution of the RNA-splicing protein muscleblind-like splicing regulator 1, elimination of foci of toxic RNA, reversal of splicing biomarkers and amelioration of myotonia. The sustained reversal of DM1 phenotypes provides further support that RNA-targeting Cas9 is a viable strategy for treating DM1 and other MRE-associated diseases.

Many eukaryotic genomes contain small repetitive 2–9 bp tracts, termed microsatellites, that serve regulatory functions. DNA repair and replication errors cause these tracts to enlarge to produce MREs that can result in cellular damage and diseases[1–11]. The diversity of the downstream pathologies associated with MREs depends on their spatiotemporal expression and is reflected by the wide range of diseases that they cause, including the most common type of adult-onset muscular dystrophy (DM1), spinal bulbar and muscular atrophy (Kennedy Disease)[12], spinocerebellar ataxias 1, 2, 3, 6, 7 and 17 (ref. [13]), oculopharyngeal muscular dystrophy[14,15], the most common type of familial amyotrophic lateral sclerosis (*C9orf72* ALS or C9-ALS)[16,17], Huntington's disease-like 2 (ref. [18]), Fuchs' corneal dystrophy[19], Huntington's disease[20] and tens of others[3].

DM1 is an autosomal-dominant inherited disorder that is characterized by CTG repeat expansions in the 3′ untranslated region of the *DMPK* gene. The repetitive RNAs produced by this locus form nuclear RNA foci[14] that sequester RNA-binding proteins such as MBNL1 (refs. [21,22]) and divert them from their homeostatic RNA-processing activities[23,24]. The loss of MBNL1 function is linked to hundreds of alternative splicing defects that cause myotonia, progressive muscle degeneration, cardiac conduction defects and respiratory insufficiency, which contribute in varying degrees to patient mortality[23,25,26]. Although DM1 was previously reported to affect 1 in 8,000 people[27] worldwide, it is now estimated that the prevalence of this devastating illness is 1 in 2,532 people[28]. DM1 is classified as either adult-onset or congenital forms, which are distinguished by the size of the expanded CTG tract.

As for all MRE diseases, available treatments address some of the symptoms of DM1 but do not target its underlying aetiology. Eliminating MREs in DNA using genome editing[7–11] could eliminate the pathogenic MREs; however, generating DNA breaks near to the repeats activates the repair machinery of which the activity is linked to expansion growth and may cause further mutation of the repeats[29]. The normally short repeat may also conduct regulatory roles in transcription[30] and DNA excision does not distinguish between the pathogenic and normal repeats[11]. Alternatively, elimination of the repetitive RNAs avoids these issues—antisense oligonucleotides[31], Cas9-mediated transcriptional inhibition[32], RNA interference using shRNAs[33] and RNA-targeting small molecules[34] have been extensively evaluated as potential DM1 therapeutics. However, these approaches require either frequent redosing (antisense oligonucleotides), penetrate affected tissues poorly (clinical trial ID: NCT02312011), do not efficiently engage repeats directly (RNA interference), may experience potential toxicity and off-target effects[35,36] and/or do not preferentially target the expanded allele[33]. An ideal therapeutic must provide long-term, efficient and specific elimination of pathogenic repetitive transcripts. We previously demonstrated that RNA-targeting CRISPR–Cas9 (RCas9) efficiently and specifically eliminates repetitive RNAs—including the CUG repeats that cause DM1—in patient-derived cellular models[37]. Motivated by the potential of a gene-therapy-based approach

[1]Department of Cellular and Molecular Medicine, University of California San Diego, La Jolla, CA, USA. [2]Stem Cell Program, University of California San Diego, La Jolla, CA, USA. [3]Institute for Genomic Medicine, University of California San Diego, La Jolla, CA, USA. [4]Locanabio, La Jolla, CA, USA. [5]Department of Molecular Genetics and Microbiology, Center for NeuroGenetics and the Genetics Institute, University of Florida, College of Medicine, Gainesville, FL, USA. [6]Department of Anesthesiology, School of Medicine, University of California San Diego, La Jolla, CA, USA. [7]Neuroregeneration Laboratory, Department of Anesthesiology, University of California San Diego, La Jolla, CA, USA. [8]These authors contributed equally: Ranjan Batra, David A. Nelles. ✉e-mail: geneyeo@ucsd.edu

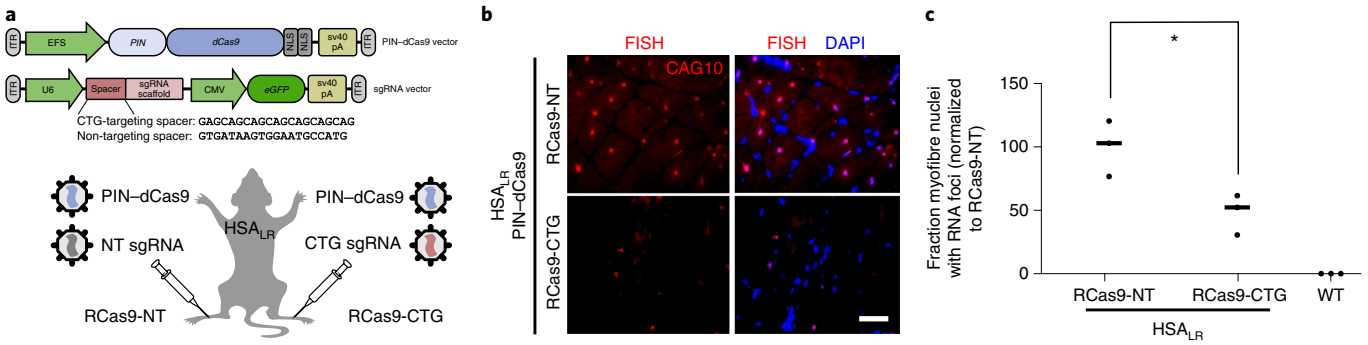

Fig. 1 | Treatment of adult skeletal muscle in the HSA_{LR} DM1 mouse model with RNA-targeting Cas9 eliminates CUG RNA foci. a, Treatment scheme for dual-vector administration of RNA-targeting Cas9 and sgRNA. A pair of vectors encoding PIN fused to nuclease-inactive Cas9 (dCas9) and either a CUG-targeting (CTG sgRNA; the resulting combination of vectors is referred to as RCas9-CTG) or non-targeting (NT sgRNA; the resulting combination of vectors is referred to as RCas9-NT) sgRNA were combined and injected into the TA of HSA_{LR} mice (aged 6–8 weeks). **b**, RNA-FISH analysis of CUG-repeat RNA in TA muscle treated with RCas9-CTG or RCas9-NT (100 nuclei were counted in 3 sections from $n=3$ mice). Scale bar, 50 µm. **c**, Quantification of the RNA-FISH analysis of the CUG-repeat RNA foci shown in **b**. Data are mean ± s.d.; $n=9$ mice with contralateral RCas9-CTG and RCas9-NT. Measurements were conducted on three serial muscle sections each. One-sided Mann–Whitney *U*-test; $U=0$, $Z=5.11$, $^*P<0.00001$.

to promote targeted, long-term treatments for genetic disease, here we evaluated the potential clinical utility of RCas9 in a predictive animal model of DM1.

To determine the therapeutic potential of RCas9 for DM1, we focused on the major clinical manifestations of the disease that are caused by the presence of CUG MRE RNA in skeletal muscle. Adult patients with DM1 experience debilitating myotonia and progressive weakness in skeletal muscle, whereas infants born with DM1 (congenital DM) are hypotonic and display respiratory insufficiency[38]. The HSA_{LR} mouse model faithfully recapitulates the skeletal-muscle-associated features of the adult disease through muscle-specific expression of 250 CTG repeats[39] and has been used extensively to characterize various anti-CUG therapeutics[23,31,40,41]. We evaluated an AAV-packaged RCas9 system targeting CUG repeats in this model through either intramuscular or systemic administration in a manner that simulates potential treatments for adult-onset disease. We addressed the ability of this approach to generate efficient and specific elimination of CUG repeats by assessing the durability of effect, molecular and physiological reversal of disease and transcriptome-wide off-target effects associated with treatment. We also assessed the effects of early neonatal treatment and transient, coadministered immunosuppression regimens on immune-tolerance induction and observed strong indications of safety over the term of the study. Overall, these safety and efficacy data indicate the potential of RCas9-based treatments for DM1 and other RNA-mediated conditions.

Results

Intramuscular injection of AAV9-packaged RCas9 eliminates CUG repeat foci and reverses hallmark splicing defects in adult DM1 skeletal muscle. To assess the potential of an RNA-targeting gene therapy for DM1, we packaged two AAV9 vectors encoding (1) nuclease-dead Cas9 (dCas9) fused to the PIN RNA endonuclease; and (2) U6-promoter-driven single-guide RNA (sgRNA)[42] with CMV-driven green fluorescent protein (GFP; Fig. 1a). The PIN–dCas9 fusion features RNA cleavage activity without DNA-cleaving activity[37] and experiments were conducted with combinations of AAV9 carrying PIN–dCas9 combined with a second AAV9 vector with either an sgRNA that does not target any sequence in the human transcriptome (non-targeting sgRNA (RCas9-NT)) or an sgRNA targeting CUG repeats (RCas9-CTG). Mice were injected with $2.5–5\times10^{10}$ vector genomes (vg) of each vector into contralateral tibialis anterior (TA) muscles of HSA_{LR} mice (aged 8 weeks) in two independent experiments[39,43] ($n=9$; Fig. 1a).

TA muscle tissue was collected 4 weeks after injection and we observed that the characteristic CUG-repeat RNA foci were efficiently eliminated by RCas9-CTG compared with RCas9-NT and contralateral saline controls, as measured using RNA fluorescence in situ hybridization (RNA-FISH) with CAG[10] probes (Mann–Whitney *U*-test; $U=0$, Z score $=5.11$, $P<0.00001$; Fig. 1b,c and Supplementary Fig. 1a,b). This in vivo result is consistent with our previous in vitro findings in cultured myotubes obtained from patients with DM1 that showed sequence-specific elimination of CUG-repeat RNA[37] by RCas9-CTG. As males have more muscle mass, females received a higher effective dose of RCas9-CTG by weight and experienced more effective elimination of CUG RNA foci (Supplementary Fig. 1b). CUG analysis using RNA-FISH and GFP immunofluorescence (CUG-sgRNA vector) of longitudinal sections (Fig. 2a) and transverse sections (Supplementary Fig. 2) distal from the injection sites in an independent HSA_{LR} cohort ($n=5$) showed that CUG RNA foci were eliminated specifically in the muscle fibres expressing RCas9-CTG.

Next, we evaluated the consequences of eliminating CUG-repeat RNA foci on characteristic downstream DM1 phenotypes. One important feature of DM1 molecular pathology is the sequestration of MBNL family proteins by CUG-repeat RNA foci[21]. We assessed MBNL1 localization in mouse muscle and observed that RCas9-CTG treatment promoted diffuse nuclear MBNL1 localization similar to wild-type (WT) mice, whereas the RCas9-NT did not correct typical foci-associated MBNL1 staining (Fig. 2b). Sequestration of MBNL protein causes alternative-splicing dysfunction of MBNL targets, such as the inclusion of exon 7a in chloride voltage-gated channel 1 (encoded by *CLCN1*)[25]. The resulting nonsense-mediated decay of *CLCN1* mRNA causes myotonia, a hallmark of DM1 (refs. [24,25,44–46]). Immunostaining analysis indicated that RCas9-CTG increased the levels of Clcn1 protein (Fig. 2c and Supplementary Fig. 1c). Consistent with this reconstitution of Clcn1 protein, PCR with reverse transcription (RT–PCR) with primers flanking exon 7a in *Clcn1* and other affected exons in *Atp2a1* (exon 22), *Tnnt3* (exon F) and *Ldb3* (also known as *Zasp* or *Cypher*, exon 11) confirmed that splicing defects were efficiently corrected in muscle treated with RCas9-CTG (Fig. 2d and Supplementary Fig. 1d; $n=9$, two independent cohorts). In addition to these molecular corrections, we also assessed the fraction of central myonuclei in muscle and observed that RCas9-CTG significantly reduced this indicator

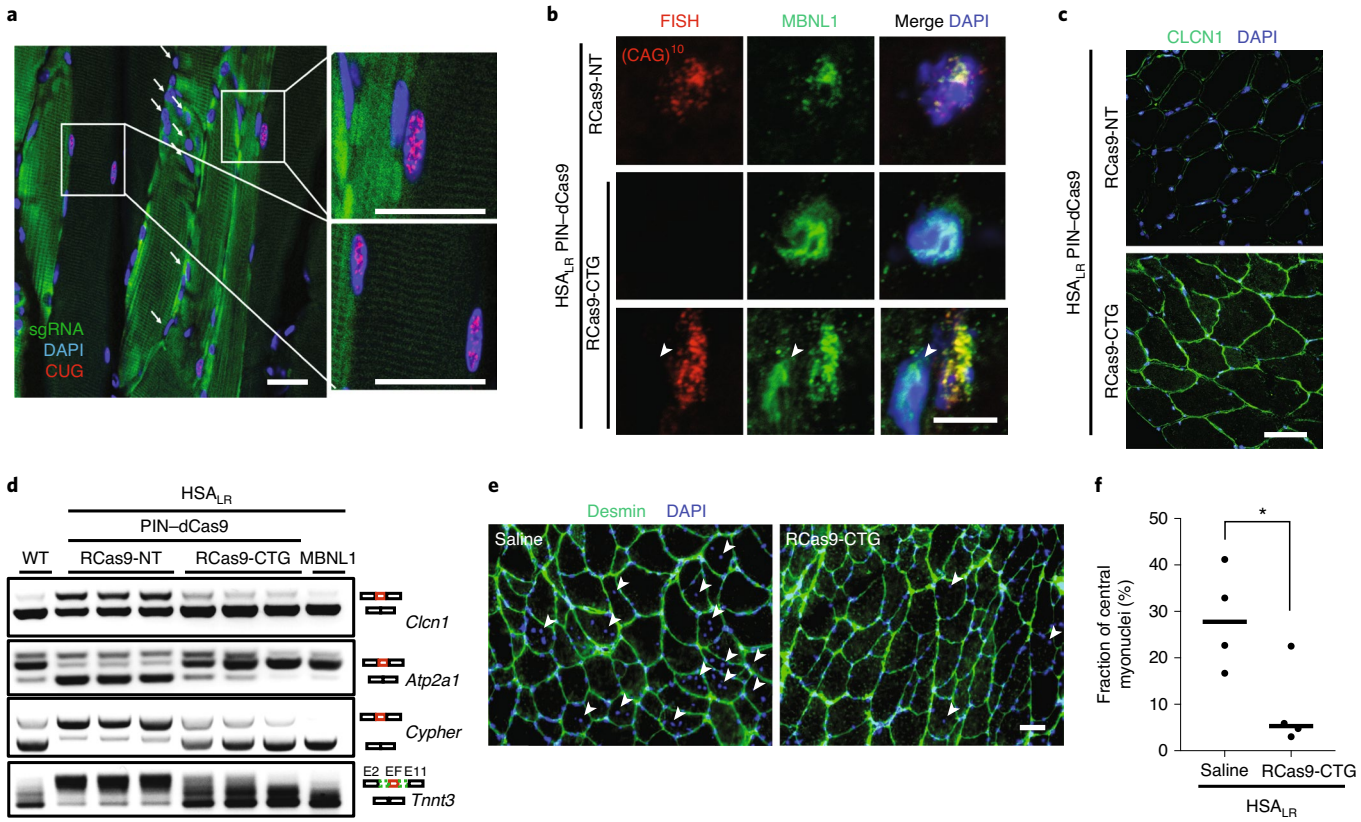

Fig. 2 | RNA-targeting Cas9 releases MBNL1 protein and reverses hallmarks of splicing dysfunction in HSA_{LR} DM1 adult muscle. a, RNA-FISH analysis of CUG repeats (red) and GFP immunofluorescence (green) of longitudinal sections of TA muscle treated with RCas9-CTG (representative image, $n=3$). Transduced cells were stained in green, whereas the adjacent dark cells lack expression of CUG-targeting sgRNA. The insets on the right highlight the presence or absence of CUG RNA foci (red). Scale bars, 50 µm. **b**, MBNL1 protein and CUG-repeat RNA foci were visualized using immunofluorescence and RNA-FISH analysis, respectively (representative image). Bottom, a pair of adjacent cells indicate diffuse MBNL1 distribution that is correlated with the absence of CUG RNA foci (white arrow), whereas focal MBNL1 is correlated with the presence of CUG RNA foci. Scale bar, 10 µm. $n=3$ mice. This experiment was reproduced in a separate cohort (Supplementary Fig. 1b) with $n=9$ mice per sex per condition. **c**, CLCN1 protein was visualized using immunofluorescence in transverse sections of TA mouse muscle in the presence of RCas9-CTG or RCas9-NT (representative image, $n=3$). Scale bar, 50 µm. **d**, Splicing of alternative exons regulated by MBNL1 (*Clcn1*, *Atp2a1*, *Cypher* (*Ldb3*) and *Tnnt3*) assessed using RT-PCR and gel electrophoresis. WT mice were compared with HSA_{LR} mice that were treated with RCas9-CTG (PIN-dCas9, CTG sgRNA), RCas9-NT (PIN-dCas9, NT sgRNA) or MBNL1-treated mice. $n=3$ mice with contralateral injections of targeting and non-targeting RCas9 systems and $n=1$ for MBNL1-treated and WT mice. **e**, The fraction of central nucleation in muscle fibres in transverse sections ($n=3$ mice) with contralateral targeting and non-targeting RCas9 systems. Scale bar, 50 µm. **f**, Quantification of central nucleation in **e**. Measurements were conducted on $n=3$ serial muscle sections each. Data are mean ± s.e.m. Statistical significance was determined using a one-tailed Student's *t*-test; $^*P=0.018$.

of muscle damage and turnover compared with the non-targeting system[47] (Fig. 2e,f; Mann–Whitney *U*-test; $U=3$, $Z=2.32$, $P<0.05$).

RCas9 reverses transcriptome-wide DM1-associated splicing defects in adult skeletal muscle. Motivated by the efficient reversal of characteristic molecular and cellular manifestations of DM1, we next expanded our analyses to transcriptome-wide measurements of RNA splicing. Broad dysfunction in RNA splicing is a central feature of DM1 and provides hundreds of semiquantitative biomarkers to assess the quality of potential therapeutics[48,49]. We performed RNA sequencing (RNA-seq) analysis of treated TA muscle of HSA_{LR} mice and observed that the alternative exon choice pattern among RCas9-CTG (10^{11} vg) clusters with MBNL1-treated mice (10^{11} vg, positive control) and vehicle-treated WT mice (Fig. 3a). MBNL1 overexpression reverses many DM1-related splicing features, providing a positive control for reversing the majority of DM1-related splicing biomarkers in skeletal muscle[23]. By contrast, splicing patterns among mice treated with AAV9 encoding RCas9-NT were distinct (Fig. 3a, Supplementary Fig. 3a,b and Supplementary Table 1). Scatter plots of percentage-spliced in (PSI, where PSI = 1 reflects complete exon inclusion) of alternatively spliced exons in HSA_{LR} and WT mice showed that splicing patterns in the presence of RCas9-CTG promotes the correction of abnormal splicing patterns (Fig. 3b, top-60 splicing changes). Overall, we found a statistically significant reversal of 86% of all DM1-related mis-splicing events (61% full reversal and 25% partial reversal; Fisher's exact test, false-discovery rate (FDR)-adjusted $P<0.05$, $dI>|0.15|$; Fig. 3b,c and Supplementary Fig. 3a,b; $n=3$ mice with contralaterally injected RCas9-CTG or RCas9-NT; top-100 splicing changes). Notably, RNA-seq analysis indicates a substantial increase in *Mef2d* exon α-2:α-1 ratio in mice treated with RCas9-CTG (and also MBNL1) compared with RCas9-NT (Fig. 3d). This key event activates the late-stage muscle differentiation program and is important for myogenesis[50,51]. Furthermore, we observed that many muscle differentiation-related genes were upregulated in RCas9-CTG and MBNL1-treated muscle (adjusted $P<0.01$; $\log_2$-transformed fold change > 2; Fig. 3e and Supplementary Table 2). Other known DM1-related splicing changes were also reversed, including *Pdlim7*

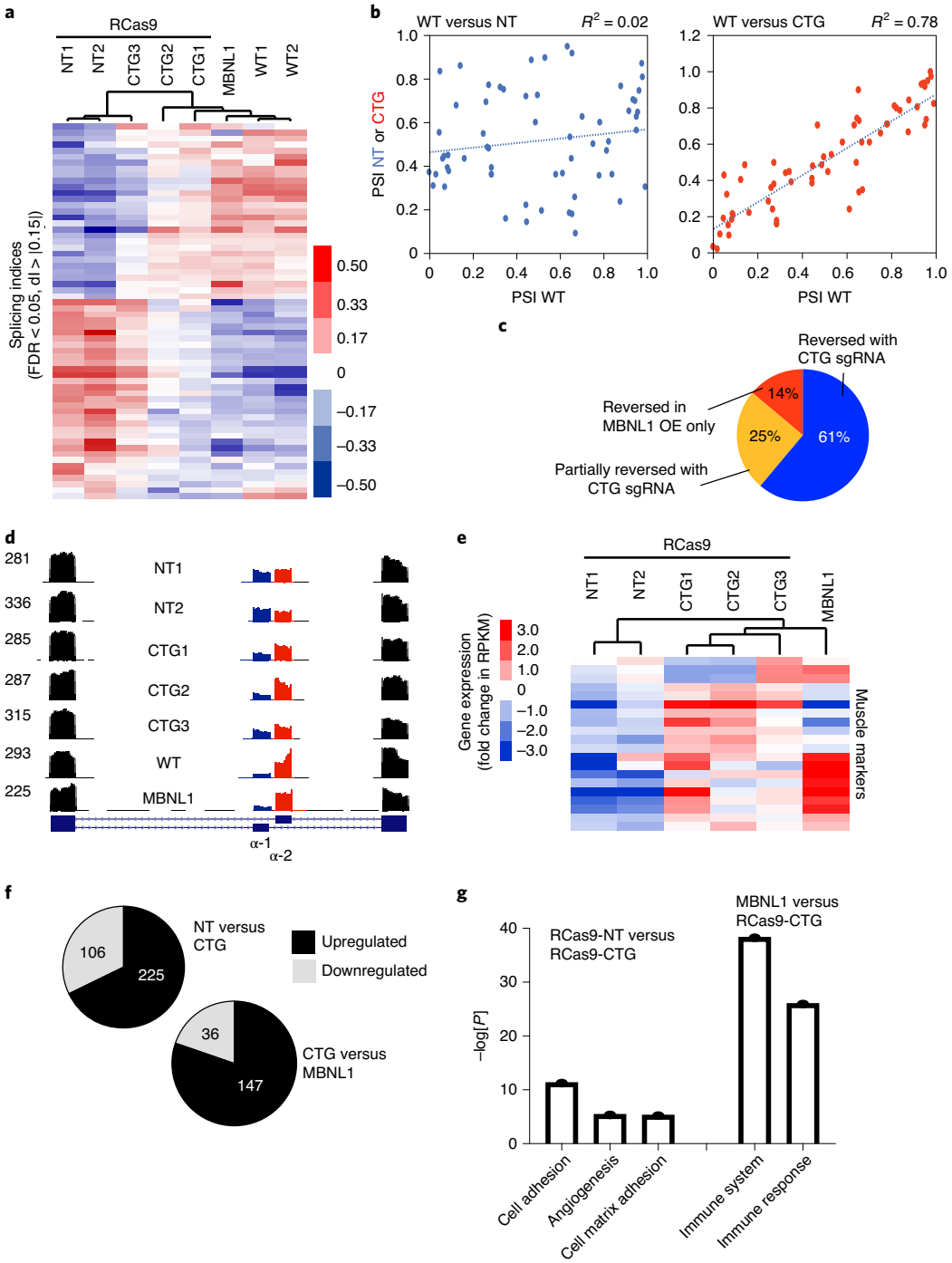

Fig. 3 | RNA-targeting Cas9 promotes a global reversal of DM1-associated splicing dysfunction and increases the expression of genes associated with proper muscle function and mature muscle. a, Hierarchical clustering (Pearson correlation) of exon inclusion indices of the genes that are most altered in HSA_{LR} TA muscle compared with the WT ($n=1$). Tissues were treated with either RCas9-CTG (CTG1, CTG2 or CTG3; $n=3$), RCas9-NT (NT1 or NT2; $n=2$) or MBNL1 protein (MBNL1; $n=1$). Each numbered sample represents a mouse. **b**, *xy* scatterplots of PSI (a measure of exon inclusion ranging from 0 to 1) between WT ($n=1$) and non-targeting (NT) ($n=2$), or between WT ($n=1$) and RCas9-CTG or CTG ($n=3$). Pearson correlation R^2 values are shown and are a measure of similarity of PSI scores between two conditions. The dotted lines represent a fitted line based on linear regression. **c**, Summary of the reversal of DM1-related alternative-splicing events describing the fraction of alternative-splicing events reversed by the RCas9 system compared with all of the splicing events regulated by MBNL1 overexpression (OE). $n=1$ (WT); $n=1$ (MBNL1); $n=3$ (RCas9-CTG). **d**, UCSC genome browser tracks of *Mef2d*, which encodes an important muscle transcription factor, demonstrating a switch from exon α-1 (fetal isoform) to exon α-2 (adult) among RCas9-CTG, RCas9-NT and MBNL1-treated mice. Each track represents $n=1$ mouse TA. **e**, Expression levels of mature muscle markers (downstream of Mef2d and myogenesis) in tissues treated with RCas9 system or MBNL1 protein OE. Each lane represents $n=1$ mouse. **f**, Gene expression changes among the mice treated with RCas9-NT (NT; $n=2$) compared with RCas9-CTG (CTG; $n=3$) and mice treated with RCas9-CTG compared with MBNL1 (positive control). Gene expression changes are summarized as either upregulated or downregulated in each of the two pairwise comparisons. **g**, GO analysis comparing RCas9-CTG (CTG-targeting) and RCas9-NT (non-targeting) or the RCas9-CTG and MBNL1 ($P<10^{-5}$). *P* values were calculated using modified Fisher's exact tests using the DAVID GO tool (https://david.ncifcrf.gov/); $-\log_{10}$-transformed *P* values are indicated.

and *Clasp1* (Supplementary Fig. 3a,c). Finally, we performed Pearson correlation and principal component analyses (PCA) to show that replicates are consistent in their splicing patterns and group together (Supplementary Fig. 3b,d,e).

We further characterized the transcriptome-wide effects of RCas9-CTG by comparing changes in gene expression level in muscle treated with RCas9-CTG, MBNL1 and RCas9-NT. Specifically, we conducted pairwise comparisons among mice treated with RCas9-NT and RCas9-CTG and mice treated with RCas9-CTG and MBNL1 and summarized gene expression changes as either upregulated or downregulated (Fig. 3f). Gene ontology (GO) analysis using DAVID[52] of changes in expression level among RCas9-CTG- and RCas9-NT-treated animals revealed that 'cell adhesion', 'angiogenesis' and 'cell-matrix adhesion' were the most statistically enriched categories (Fig. 3g and Supplementary Table 3). Defects among these phenomena are linked to DM1 (refs. [26,53]). Furthermore, Pearson correlation analysis of gene expression shows that there is a greater correlation in gene expression between the RCas9-CTG- and MBNL1-treated animals compared with between the RCas9-NT-treated and WT mice (Supplementary Fig. 3f), and replicates showed low variability. We also addressed the specificity of RCas9-CTG by measuring levels of genes that feature small CUG repeat tracts. For example, RNA levels of *Dmpk* were not affected by RCas9-CTG treatment (Supplementary Figs. 3g and 7a and Supplementary Table 2e).

Delivery of RCas9 to adult muscle induces expression of immune-response-linked genes but causes no overt muscle damage. Many CRISPR-based gene therapies involve long-term expression of non-self, potentially immunogenic Cas proteins. To assess whether the presence of RCas9 in muscle causes a damaging immune response, we compared the immune response of HSA_{LR} mice that were treated with AAV9 encoding either RCas9-CTG or mouse MBNL1. GO analysis of gene expression revealed upregulation of genes linked to the major histocompatibility complex I (MHC-I), antigen presentation and T-cell response pathway, but not MHC-II (Fig. 3g and Supplementary Figs. 4 and 5). We conducted histological analysis of RCas9-CTG-treated TA (haematoxylin and eosin (H&E) staining) and observed no substantial alterations in muscle morphology (Supplementary Fig. 1e). As a metric for immune-response-linked muscle damage, we measured the degree of central myonucleation in muscle fibres in HSA_{LR} mice and observed that treatment with RCas9-CTG significantly reduced this marker of damage compared with untreated mice (Fig. 2e,f).

Pharmacological immunosuppression or Cas9 protein pre-treatment promotes sustained RCas9-CTG expression in adult muscle. By avoiding the use of DNA nucleases, RNA-targeting approaches avoid risks associated with off-target genome edits[37,54,55]. However, in contrast to genome editing approaches, RNA-targeting enzymes must be present in diseased cells to continuously engage pathogenic RNAs as they are transcribed. One major concern with non-self-proteins, such as Cas9, is the adaptive immune response. We treated WT mice with FDA-approved immunosuppressors tacrolimus and a fusion protein of CTLA-4 and immunoglobulin antibodies (CTLA4-Ig or abatacept, which prevents T-cell activation by targeting CD80 and CD86) for 2 weeks after AAV administration—which inhibit T-cell proliferation and costimulation, respectively[56]—to determine whether these FDA-approved immunosuppressants contribute to stable and, therefore, sustained expression of RCas9-CTG ($n=4$ mice per group, total of 16 mice). Cytotoxic adaptive immune response to treated cells is known to peak at 4 weeks after administration[57] but we observed prolonged expression of RCas9-CTG levels at timepoints up to 12 weeks in both untreated and immunosuppressed groups. Mice treated with both immunosuppressants displayed modestly higher levels of Cas9 expression at 12 weeks after injection (Fig. 4a; paired Student's *t*-test, 1.75-fold, $P<0.001$). At 1, 6 and 12 weeks after injection, we observed that transcriptome-wide gene expression clusters by age and not by treatment, indicating that immune response and off-target effects are probably not the primary drivers of gene expression changes (Fig. 4b). Furthermore, we did not observe any gene expression changes (adjusted $P<0.01$) between non-immunosuppressed and immunosuppressed groups (Supplementary Table 4c). We observed no overt tissue damage and only occasional nests of $CD3^+$ T cells in RCas9-CTG-treated muscle 4 weeks after injection, whereas the mice with combined immunosuppression (tacrolimus and CTLA4-Ig) showed no $CD3^+$ T-cell nests (Fig. 4c). Overall, these findings indicate that transient immunosuppression could increase transduction and/or prevent a low-level cytotoxic immune response to treated cells.

Skeletal muscle dystrophy is associated with inflammatory markers[58]. Indeed, IL-6 and TNFα are elevated in patients with DM1 (refs. [59–61]). Furthermore, Celf1 upregulation and *Mbnl1* knockout mouse models of DM1 show immunological problems[62,63]. Pre-existing inflammation in DM1 muscle may amplify the immune response to therapeutics. To investigate this phenomenon in HSA_{LR} muscle, we compared the following experimental groups (all intramuscular injections in TA muscle): (1) HSA_{LR} mice treated with saline ($n=4$); (2) WT mice treated with RCas9-CTG ($n=5$); (3) HSA_{LR} mice treated with RCas9-CTG ($n=4$); and (4) HSA_{LR} mice treated with RCas9-CTG and transient immunosuppression ($n=4$, tacrolimus and CTLA4-Ig for 2 weeks after injection). We observed high levels of T-cell infiltration in group 3 (Figs. 4d and 5a and Supplementary Fig. 6a; $P<0.01$), indicating that pre-existing inflammation in DM1 muscle may potentiate the recognition of Cas9 and clearance of treated cells by the adaptive immune system. Consistent with a cytotoxic immune response to treated cells, we observed serial reductions in RCas9-CTG expression at 8 and 12 weeks after injection. This effect was eliminated by immunosuppression; mice in group 4 were indistinguishable from mice treated with saline (group 1; Fig. 5a) and robust RCas9-CTG expression was observed at 8 and 12 weeks (Fig. 5b). This result indicates that durable expression of RCas9 is possible with approved immunosuppressants, even in an inflamed niche.

Whereas transient immunosuppression seems to promote sustained expression of RCas9 in adult mice, another strategy utilizes the developing immune system in neonatal mice to induce tolerance to immunogenic peptides. Specifically, we assessed whether exposure to RCas9 antigens in neonatal mice could promote durable expression in adult mice treated with RCas9-CTG. We treated neonatal (P0) mice systemically (temporal vein) with 0 ng, 100 ng or 250 ng of purified recombinant dCas9 protein followed by intramuscular injection of RCas9-CTG at 4 weeks. We observed decreased *HSA* CUG levels (Supplementary Fig. 6b) and increased *Cas9* expression, on the basis of quantitative PCR (qPCR), in the muscle of protein-treated mice (Supplementary Fig. 6c).

RNA measurements indicate sustained specificity for long CUG repeats. To address the specificity of RNA-targeting CRISPR, we assessed whether genes containing short tracts of CTG repeats are affected by RCas9-CTG. In the TA muscle of WT mice treated with RCas9-CTG, we measured the mRNA expression levels of 115 genes containing short CTG repeat (>6 repeats) tracts using RNA-seq and did not observe any differences in expression of these genes compared to sgRNA treatment alone (Supplementary Table 4 and Supplementary Fig. 7a). At time points up to 12 weeks, transcriptome-wide analysis on the basis of gene expression values ($\log_2$-transformed reads per kb of transcript per million mapped reads (RPKM)), hierarchical clustering (Fig. 4b), correlation (Supplementary Fig. 7b) and PCA (Supplementary Fig. 7c) grouped the samples by time after infection rather than by treatment.

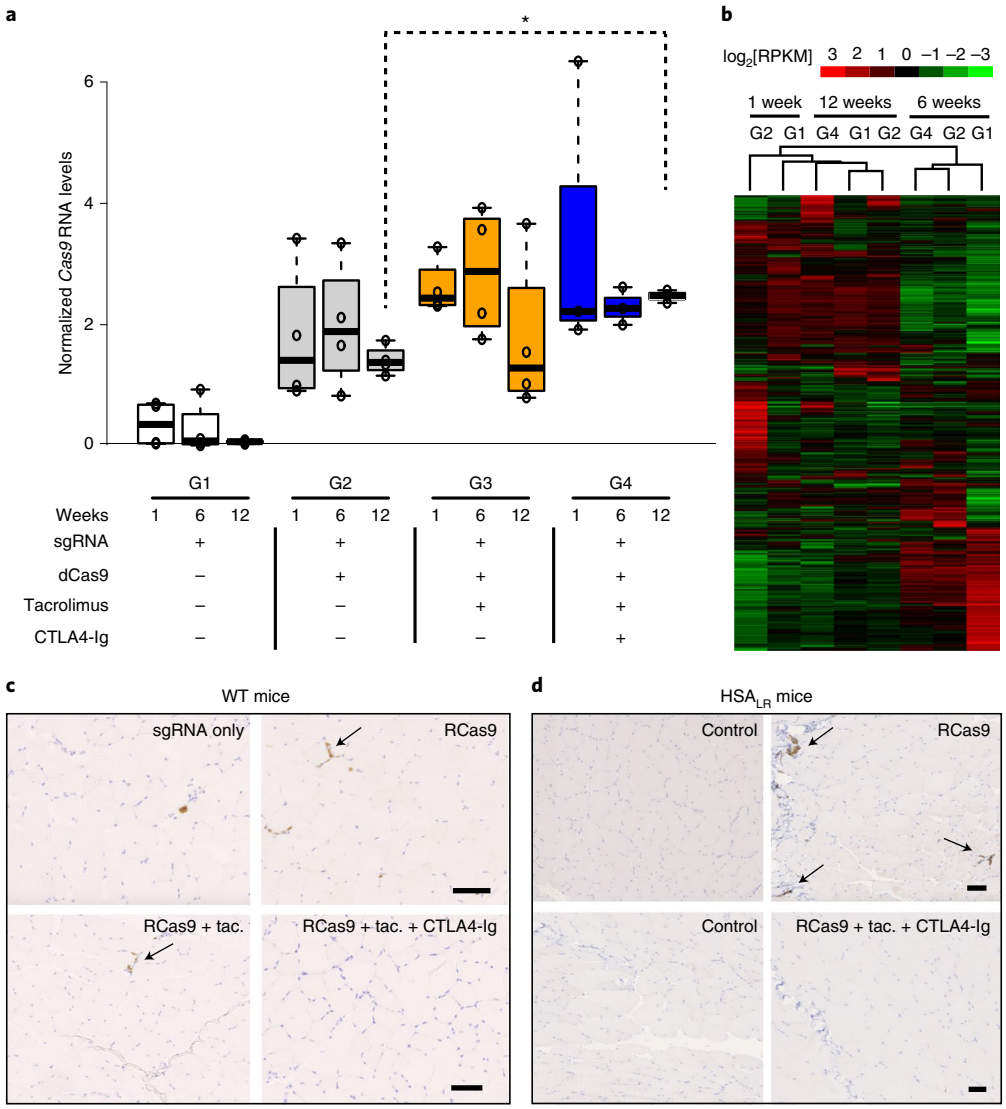

Fig. 4 | Sustained expression of RNA-targeting Cas9 in WT adult muscle. a, *Cas9* mRNA levels in TA muscle of WT mice treated with AAV9 encoding PIN-dCas9 and sgRNA as assessed by RT-qPCR at 1, 6 and 12 weeks after treatment. Mice were treated with various immunosuppression regimens transiently for 2 weeks. Interquartile range and median as indicated were determined with $n=4$ mice per condition per time point for a total of 48 mice. Statistical analysis was performed using a two-tailed paired Student's *t*-test; 1.75-fold, $^*P=0.00055$. The centre lines show the median values, the box limits indicate the 25th and 75th percentiles as determined using R and the whiskers extend to 1.5× the interquartile range from the 25th and 75th percentiles; outliers are represented by dots. **b**, Hierarchical clustering (Pearson correlation) of $\log_2$[RPKM] of the most altered genes in WT mice 1, 6 and 12 weeks after treatment injected into the TA with sgRNA alone (G1), sgRNA and PIN-dCas9 (G2), or sgRNA, PIN-dCas9, tacrolimus and CTLA4-Ig (G4). The groups are the same as described in Fig. 3a. Each lane represents $n=1$ mouse TA. **c**, $CD3^+$ immunohistochemistry analysis of T cells in WT mice that were treated with sgRNA only, PIN-dCas9 and sgRNA (RCas9), PIN-dCas9 and sgRNA with tacrolimus (RCas9 + tac.), or PIN-dCas9 with tacrolimus and CTLA4-Ig (RCas9-CTG + tac. + CTLA4-Ig) 4 weeks after injection (representative images, $n=4$). T-cell nests are indicated by black arrows. Scale bars, 50 μm. **d**, $CD3^+$ immunohistochemistry analysis of T cells in HSA_{LR} mice treated with either control (AAV9 with empty filler genome, injected into the left TA) or RCas9-CTG (RCas9, injected into the right TA), with or without tacrolimus and CTLA4-Ig (RCas9 + tac. + CTLA4-Ig) 4 weeks after injection (representative images, $n=4$). Scale bars, 50 μm.

These results indicate that off-target effects of RCas9 are not the major distinguishing factor between mice treated with RCas9-CTG or NT sgRNA only.

Correction of DM1-associated abnormalities by systemic administration of RCas9 in neonatal and adult HSA_{LR} mice. We next investigated whether systemic treatment in either neonates or adults with RCas9-CTG can reverse the molecular and physiological features of DM1. We conducted a pair of systemic treatment studies in either neonatal mice (temporal vein; Supplementary Fig. 8a; $n=6$) or adult mice (lateral tail vein, coadministered with tacrolimus and CTLA4-Ig, as described in Fig. 5b; $n=3$). Mice were injected with either RCas9-CTG (2×10^{11} vg total vector for each neonate or 1×10^{12} vg total vector for each adult, equal amounts of AAV9 encoding either PIN–dCas9 or sgRNA), saline (neonatal) or vehicle control (adults) in HSA_{LR} mice. RCas9 levels were sustained in the quadriceps and TA muscles up to 16 weeks (Fig. 6a and Supplementary Fig. 8b,c; Student's *t*-test, $P<0.01$). To assess the efficiency of CUG-repeat RNA elimination, we measured HSA_{LR} transgene RNA levels as a proxy for CUG-repeat RNA levels

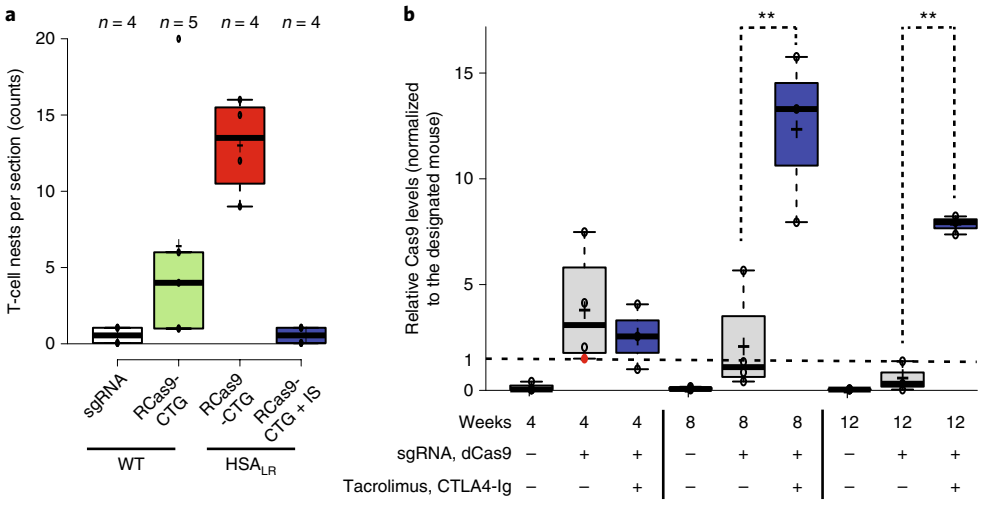

Fig. 5 | Transient pharmacological immunosuppression promotes sustained expression of RNA-targeting Cas9 in adult muscle. a, Quantification of Fig. 4c,d. $n=4$ or $n=5$ mice. Genotypes were labelled at 4 weeks after injection. The lanes represent sgRNA-alone control (WT), RCas9-CTG (WT), RCas9-CTG (HSA_{LR}) and RCas9-CTG cotreatment with transient immunosuppression (IS) with tacrolimus and CTLA4-Ig. The centre lines show the median values, the box limits indicate the 25th and 75th percentiles as determined using R and the whiskers extend to 1.5× the interquartile range from the 25th and 75th percentiles; outliers are represented by dots. **b**, RCas9-CTG RNA levels in TA muscle of HSA_{LR} mice that were treated with AAV9 encoding PIN-dCas9 and sgRNA, as assessed using RT-qPCR. HSA_{LR} mice were treated with control (AAV9 with empty filler genome, injected into the left TA) and either RCas9-CTG (RCas9) or RCas9-CTG (RCas9) with tacrolimus and CTLA4-Ig (RCas9-IS) for 4, 8 and 12 weeks. $n=4$. Two-tailed Student's *t*-tests, $^{**}P=0.0079$ (8-week samples RCas9-CTG versus RCas9-CTG + immunosuppression); $^{**}P=0.0000543$ (12-week samples RCas9-CTG versus RCas9-CTG + immunosuppression). One-tailed Student's *t*-test, $P=0.125$ (8-week RCas9-CTG + immunosuppression versus 12-week RCas9-CTG + immunosuppression). The centre lines show the median values, the box limits indicate the 25th and 75th percentiles as determined using R and the whiskers extend to 1.5× the interquartile range from the 25th and 75th percentiles; outliers are represented by dots.

and observed significant decreases in RCas9-CTG-treated neonatal mice (Fig. 6a and Supplementary Fig. 8b,c; Student's *t*-test, $P<0.05$). For adult mice, we assessed the RNA levels of RCas9 as well as GFP as a proxy for sgRNA in disease-relevant tissues, such as the TA, quadriceps, diaphragm and heart using qPCR at 4 and 8 weeks after injection (Fig. 6b). We also measured RCas9 levels in the liver (Supplementary Fig. 9a,b). We observed previously reported distribution patterns[64], including an increase in transgene expression in the liver compared with cardiac and skeletal muscles (Supplementary Fig. 9a,b). Importantly, both Cas9 and GFP (correlated with sgRNA) RNAs were simultaneously detected in most of these tissues[65,66] (Fig. 6b and Supplementary Fig. 9a,b). We also observed a decrease in the number of CUG RNA foci (Fig. 6c,d; $n=3$; $P<0.005$) and HSA_{LR} transgene RNA levels (Fig. 6e; $n=3$; $P<0.05$) in the quadriceps muscle of RCas9-CTG-treated adult mice. Furthermore, we also observed a reversal in the *Atp2a1* (exon 22) and *Clcn1* (exon 7a) splicing patterns to the WT patterns in the quadriceps of mice that were treated both as neonates and adults (Fig. 6f and Supplementary Fig. 8d,e). Finally, we performed a liver enzyme panel and observed no elevation in the levels of liver enzymes despite high expression of RCas9-CTG in the liver (Supplementary Fig. 10a).

We next measured the efficacy of our therapeutic in terms of physiological and functional manifestations of disease. Myotonia can be assessed in HSA_{LR} mice on the basis of the latency between hindlimb flexing and relaxation. Hindlimb pull-test measurements revealed that control-treated HSA_{LR} mice displayed typical myotonia, whereas both P0 (measured at both 8 and 16 weeks after injection) and adult (measured at 4 weeks after injection) HSA_{LR} mice treated with RCas9-CTG displayed reduced myotonia ($n=6$ for P0, $n=3$ for adults; Fig. 7a and Supplementary Videos 1 and 2; Mann–Whitney *U*-test; $U=0$, $Z=2.8$, $P<0.01$). Electromyography measurements revealed a significant decrease in the percentage of myotonic runs after needle electrode insertion in RCas9-CTG-treated mice compared with the controls ($n=5$ for P0 and $n=3$ for adults; Fig. 7b,c; Mann–Whitney *U*-test; $U=0$, $Z=2.8$, $P<0.01$). Overall, these data indicate that expression of RCas9-CTG after systemic administration can cause both efficient and sustained reversal of physiological manifestations of the disease.

Discussion

RNA-targeting CRISPR technologies show promise for addressing a wide range of genetic diseases without the risk of off-target genome editing[37,54,55], but the in vivo safety, durability and efficacy of these approaches have not been tested to date. We address these questions in the context of a DM1 mouse model using an AAV9-packaged RCas9 system. Overall, our results indicate that RCas9 treatment in conjunction with transient immunosuppression promotes sustained and specific therapeutic activity through both local and systemic treatment modes in adult and neonatal mice.

Myotonic dystrophy is a multisystemic disorder and the age of onset and severity depends on the number of expanded CTG repeats. We previously demonstrated that RCas9 specifically binds to and eliminates expanded CUG-repeat-containing RNAs resulting in the reversal of the molecular features of this disease in human cells[37]. Here we utilized a mouse model that expresses 250 CUG repeats driven by the human skeletal actin *ACTA1* promoter (HSA_{LR} model) as an established preclinical model of DM1 (refs. [33,39]). Both systemic and intramuscular administration of RCas9-CTG resulted in the reversal of disease-linked splicing defects to resemble WT patterns. Indeed, MBNL protein sequestration by CUG repeats is linked to splicing dysfunction and we observed its release from CUG RNA foci. Overall, these results are consistent with our findings in patient myotubes and indicate potent CUG-repeat RNA elimination in vivo. To further investigate the clinical potential of this approach, we studied the safety and durability over time of this RCas9 system.

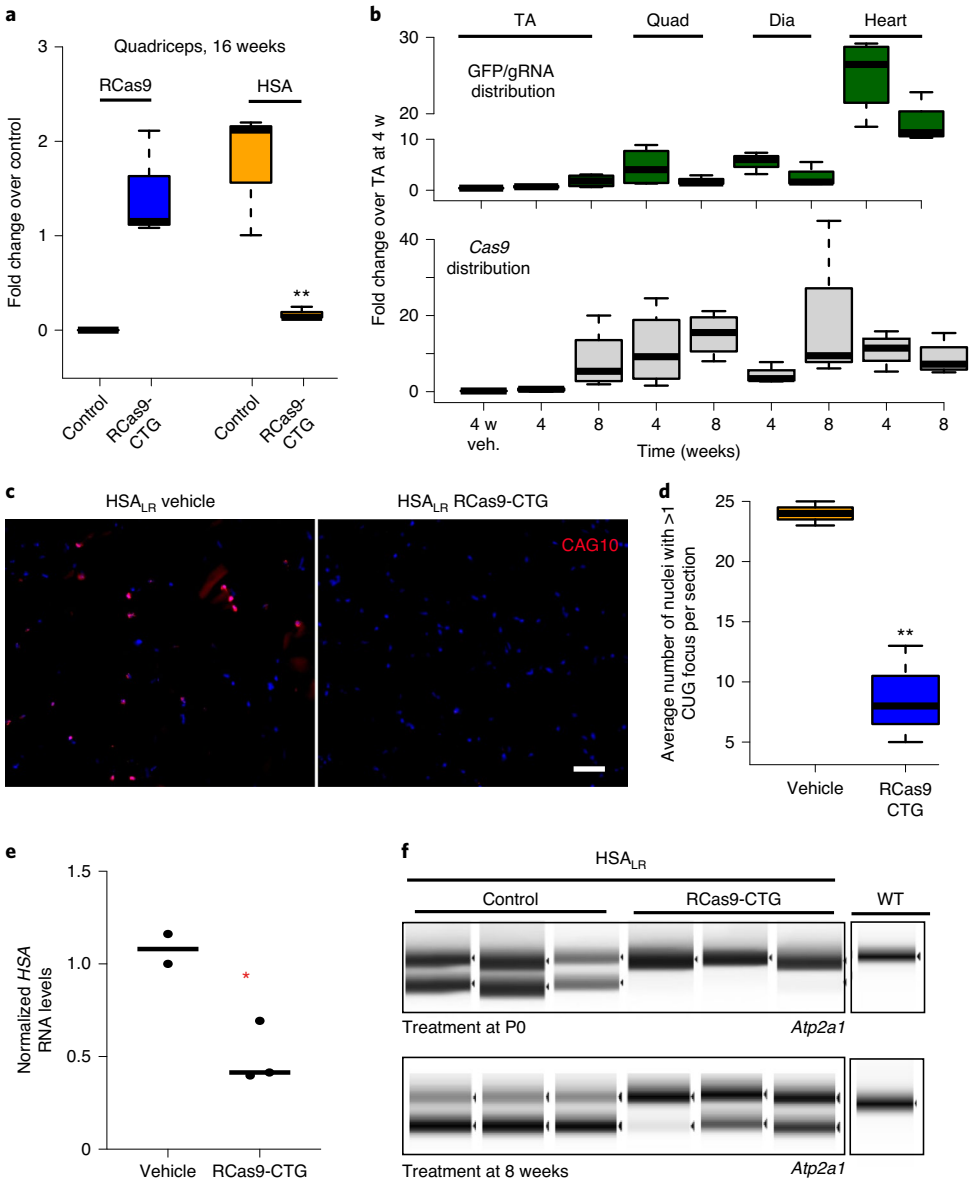

Fig. 6 | Systemic treatment of HSA_{LR} DM1 mice with RNA-targeting Cas9 leads to sustained expression in various tissues, eliminates toxic RNA foci and reverses DM1-related mis-splicing. a, mRNA levels of *Cas9* (blue) and HSA_{LR} (CUG repeat levels, orange) in the quadriceps muscle of mice that were treated with either control or RCas9-CTG 16 weeks after treatment with 2×10^{11} vg of AAV9-RCas9-CTG in P0 (neonatal) HSA_{LR} mice. $n=3$ for each condition. Statistical significance was determined using a one-tailed Student's *t*-test; $^{**}P=0.0071$. The centre lines show the median values, the box limits indicate the 25th and 75th percentiles as determined using R and the whiskers extend to 1.5× the interquartile range from the 25th and 75th percentiles; outliers are represented by dots. **b**, The distribution of mRNA levels of GFP gRNA (green) and *Cas9* (grey) levels in various indicated tissues measured using RT–qPCR at 4 and 8 weeks after lateral tail vein injection of 1×10^{12} vg of AAV9-RCas9-CTG vectors in adult (aged 8 weeks) HSA_{LR} mice ($n=3$). The levels were normalized to the levels in TA muscle at 4 weeks. 4 w veh., vehicle treatment at 4 weeks. The centre lines show the median values, the box limits indicate the 25th and 75th percentiles as determined using R and the whiskers extend to 1.5× the interquartile range from the 25th and 75th percentiles; outliers are represented by dots. **c**, RNA-FISH analysis of CUG-repeat RNA in the quadriceps muscle 4 weeks after lateral tail vein injection of either vehicle control or 10^{12} vg of AAV9-RCas9-CTG (100 nuclei were counted in 3 sections from $n=3$ mice) in adult HSA_{LR} mice (aged 8 weeks). Scale bar, 50 µm. **d**, Quantification of RNA-FISH analysis of CUG-repeat RNA foci in adult HSA_{LR} mice (aged 8 weeks) in **c**. Statistical significance was determined using a one-tailed Student's *t*-test; $^{**}P=0.0015$. $n=3$ each. The centre lines show the median values, the box limits indicate the 25th and 75th percentiles as determined using R and the whiskers extend to 1.5× the interquartile range from the 25th and 75th percentiles; outliers are represented by dots. **e**, *HSA* RNA levels in the quadriceps muscle 4 weeks after lateral tail vein injection of either vehicle control or 10^{12} vg of AAV9-RCas9-CTG in adult HSA_{LR} mice (aged 8 weeks). $n=3$. Statistical significance was determined using a one-sided Student's *t*-test; $^{*}P<0.024$. **f**, Splicing of alternative exon 22 in *Atp2a1* assessed using RT–PCR in quadriceps 16 weeks after temporal vein injection of P0 (neonatal) HSA_{LR} mice with either saline or 10^{11} vg of AAV9-RCas9-CTG (top). Splicing of alternative exon 22 in *Atp2a1* was assessed using RT–PCR in the quadriceps 4 weeks after lateral tail vein injection of adult HSA_{LR} mice (aged 8 weeks) with either vehicle or 10^{12} vg of AAV9-RCas9-CTG (bottom). Total $n=3$ mice for each condition, each lane represents measurements from a single mouse.

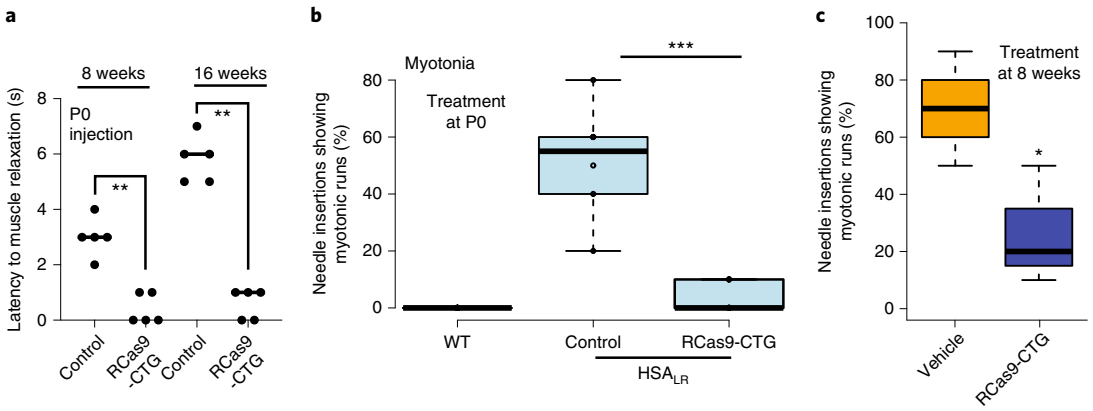

Fig. 7 | Systemic treatment of HSA_{LR} DM1 mouse model with RNA-targeting Cas9 reverses behavioural and electrophysiological features of the disease. a, Quantification of pull-test measurements in terms of latency (seconds) to hind-limb relaxation at 8 and 16 weeks after treatment of P0 (neonatal) HSA_{LR} mice with either saline (control) or 10^{11} vg of AAV9-RCas9-CTG. $n=5$. One-sided Mann–Whitney *U*-test; $U=0$, $Z=2.5$, $^{**}P=0.0064$. Each dot represents an individual mouse. **b**, Electromyography of TA of untreated WT, treated control (saline) and AAV9-RCas9-CTG-treated (10^{11} vg) P0 (neonatal) HSA_{LR} mice at 8 weeks after temporal vein injection. $n=5$ mice for each condition. One-sided Mann–Whitney *U*-test; $U=0$, $Z=2.8$, $^{***}P=0.00256$. The centre lines show the median values, the box limits indicate the 25th and 75th percentiles as determined using R and the whiskers extend to 1.5× the interquartile range from the 25th and 75th percentiles; outliers are represented by dots. **c**, Electromyography of TA of adult HSA_{LR} mice (aged 8 weeks) 4 weeks after lateral tail injection of either vehicle or AAV9-RCas9-CTG (10^{12} vg). $n=3$ mice for each condition. The centre lines show the median values, the box limits indicate the 25th and 75th percentiles as determined using R and the whiskers extend to 1.5× the interquartile range from the 25th and 75th percentiles. Statistical significance was determined using a one-tailed Student's *t*-test; $^{*}P=0.03$.

An important safety metric is specificity. For an RNA-targeting therapy, off-target effects can be quantitatively and comprehensively assessed using RNA-seq technology. The source of RNA off-target effects fall into two broad categories: (1) off-target effects associated with aberrant behaviour of the therapeutic itself; and (2) indirect off-target effects due to titration of host cellular machinery by the therapeutic agent. The most probable source of off-target effects in the first category could occur among transcripts with short, non-pathogenic CUG repeat tracts, but we observed no such activity. The observed specificity for long, pathogenic repeats may be due to the relatively slow cleavage kinetics that are associated with the PIN endonuclease such that multiple binding events on a long target site are required for efficient cleavage[67]. The second category constitutes indirect off-target effects that are inherent to approaches such as RNA interference or gapmer antisense oligonucleotides that require host cellular machinery to cleave target RNAs. RCas9 is enzymatically self-contained and neither requires nor competes for endogenous enzymes for its activity. By contrast, RNA silencing using short interfering RNAs (siRNAs) or antisense gapmers can cause dysregulation of important biological processes that require the RISC complex or RNase H, such as microRNA-mediated post-transcriptional gene expression regulation or the removal of RNA primers from Okazaki fragments during DNA replication[68], respectively. Overall, the choice of enzymes utilized within the RCas9 system could provide future opportunities to further refine on- and off-target activity to match the target indication.

Therapeutic safety in muscle is assessed in terms of histological manifestations of tissue turnover and immune response. DM1-associated muscle dysfunction leads to the presence of centralized myonuclei in the DM1 mouse model[39]. The fraction of central myonuclei indicates both muscle damage (increased numbers of central myonuclei) caused by the therapeutic or therapeutic reduction (decreased numbers of central myonuclei) of muscle turnover. Here the decrease in central myonuclei reveals that RCas9-CTG does not cause overt muscle damage and, in fact, reverses this disease pathology. As further support, the corrected splicing pattern of *Mef2d*, which encodes a transcription factor, and upregulation of mature muscle markers are consistent with proper muscle differentiation and reduced turnover. Together, these results indicate that RCas9-mediated elimination of toxic RNA leads to an overall improvement in muscle health.

Gene therapies for muscle diseases involve the administration of therapeutics to large tissue volumes, which can potentiate unwanted immune response to the treatment. Recent clinical trials involving AAV for genetic muscle diseases[69] (ASPIRO trial NCT03199469 for XLMTM; SRP4045 trials NCT02530905 and NCT03769116 for DMD) indicate the potential for safe, systemic gene therapies. The first in vivo clinical trial by Editas and Allergan will shed light on the safety of Cas9 (NCT03872479), but it remains to be seen whether the long-term and widespread expression of bacterial Cas proteins is tolerated through systemic and local muscle delivery. The issue of anti-therapeutic immune response is reinforced by the fact that disease-mediated tissue degeneration can cause local inflammation and prime the immune system to recognize and attack therapeutic antigens (Cas proteins). This issue is made clear in our comparison of RCas9-CTG-treated WT and HSA_{LR} DM1 mice. HSA_{LR} muscle displays greater T-cell infiltration and reduced Cas9 expression at 12 weeks after intramuscular injection of RCas9-CTG. By conducting transient immunosuppressive cotreatment in the diseased mice, we were able to eliminate this response in a manner that was effective for the length of the study and promoted sustained levels of the therapeutic system, indicating that durable expression of RCas9-CTG is possible with approved immunosuppressants, even in an inflamed niche. Further studies are required to assess the precise mechanism(s) and antigens that mediate the recognition of Cas9 by the adaptive immune system. A recent study reported human T-cell immunity against *Streptococcus pyogenes* Cas9 and found dominant *Sp*Cas9 peptides that are displayed by MHC-I and elicit a T-cell response in donor peripheral blood mononuclear cells[70]. However, our study and previous studies[56] indicate that transient immunosuppression typically used in conjunction with AAV administration (clinical trials: NCT03199469 and NCT0376911) is sufficient to promote sustained transgene expression in mice without overt adverse immunological effects. There is also growing evidence that the expression of therapeutic transgenes at specific times in development[71] or specific tissues[72–74] can be sufficient to induce tolerance to the transgene. Consistent with these studies, we observed sustained Cas9 expression in adult mice that were exposed

to Cas9 as neonates. These results reveal a second route to sustained RCas9 expression in large tissue volumes in mice. Translation of these findings to humans will require studies in larger animal models to identify proper AAV9 dosing, administration methods and specific immunosuppression regimens.

Indeed, dose escalation studies are an important aspect of preclinical drug development. The dose should fall within a therapeutic window with sufficient distinction from the toxicity threshold to reduce the risk of adverse effects. The therapeutic index (TI) is defined as the ratio of a toxic dose to an effective dose, such that larger TI values indicate safer treatments. The dearth of approved gene therapies provides a limited basis to compare TI values or to choose dose ranges for dose finding studies. Recent approved therapies (ZOLGENSMA) and clinical trials using intravenous gene therapy with AAV have used doses from 1×10^{14} to 3×10^{14} vg per kg (NCT03199469 with AAV8, NCT03362502 with AAV9). Our studies involved dose ranges in mice from $2.5–5\times10^{13}$ vg per kg, which promoted the reversal of disease phenotypes at levels of twofold to fourfold lower than the lowest vector dose used in the aforementioned trials. Importantly, in contrast to an increase in liver enzymes that was observed in animal models treated with Novartis' ZOLGENSMA (1.1×10^{14} vg per kg, see package insert), we observed no elevation of liver enzymes in mice in our studies. These findings highlight the promise that systemically delivered AAV9-RCas9-mediated CUG-repeat elimination in DM1 may provide clinical efficacy while staying considerably below the toxic dose ranges of gene therapy. Future research in larger animal models will clarify the safety at various doses of AAV9-RCas9-CTG.

Since the publication of our initial research describing the repurposing of Cas9 to target RNA[75], a host of RNA-specific Cas proteins have been described in the literature[54,55,76,77]. These proteins are typically smaller than *Sp*Cas9 and could be packaged in a single AAV9 vector with a sgRNA, which could reduce the AAV dose and therapeutic cost, although the relative ability of these proteins to engage repetitive RNAs is not yet known. In conclusion, our study indicates the potential of RCas9 and potentially other RNA-targeting CRISPR-based approaches to address disease. Advancement of this approach to patients will depend on future studies in large animals to further assess the safety, dose levels and immunosuppression regimens that are required for safe and long-term treatments.

Methods

Transgenic mice. HSA_{LR} transgenic mice were used for this study[39]. Tail clips were taken from the pups at weaning and genomic DNA was extracted by heating the tail clips at 50 °C at 500 r.p.m. in lysis buffer (100 mM Tris pH 8.5, 200 mM NaCl, 5 mM EDTA, 0.2% (w/v) SDS) mixed with 5 µl proteinase K (10 mg ml^{-1}) in a thermomixer. Genotypes were determined by a PCR reaction using the primers HSA-LR forward 5′-CGGCTGAGCTCCAGCCACCCCGCAGTC-3′ and HSA-LR reverse 5′-AATGCTTCTTCAAGTTTTCCATTTTCT-3′. Intergenerational stability of the $(CTG)_{250}$ expansion was monitored using PCR around the repeat locus. All of the mice used in this study had >200 repeats, as estimated by the size of the band.

rAAV9 construct and virus preparation. We generated ssAAV2/9 to deliver our RCas9 vectors. The dCas9-2xNLS (nuclear localization signal) sequence was derived from pHR-SFFV-dCas9-BFPKRAB (a gift from S. Qi and J. Weissman; Addgene plasmid, 46911), tagged with two SV40 NLS sequences on the C terminus and fused to PIN on the N terminus. This fusion was placed into pAAV-CMV-GFP (digested with NotI; a gift from J. Gray, Addgene plasmid, 32395) with an EFS promoter (derived from lentiCRISPR v2, a gift from F. Zhang, Addgene plasmid, 52961) and terminated with an SV40 polyadenylation signal (derived from pCDNA 3.1, Life Technologies) using Gibson assembly. The sgRNA AAV vector was assembled as previously described[75] and placed into the NotI-digested pAAV-CMV-GFP vector by Gibson assembly. Helper virus-free rAAV9 vectors expressing either PIN–dCas9 or sgRNA were produced by transient transfection of HEK293T cells with the vector plasmid pRep2-Cap9 and pAd-helper plasmid. The plasmid pRep2-Cap9 was obtained from the Vector Core at the University of Pennsylvania. AAV vectors in the cell lysates prepared 72 h after transfection were purified by a combination of anion-exchange column chromatography and ultracentrifugation and titred using qPCR[78]. AAV9 with filler genome is an AAV9 capsid carrying an AAV genome within the AAV2 inverted terminal repeats carrying a non-vertebrate, non-specific sequence. The MBNL1 AAV9 vector was prepared using the HEK293 triple-transfection method at University of California San Diego Vector Core. The plasmid carrying MBNL1 (pTR-UF12Δ-mycMbnl1/41) was described previously by Kanadia et al.[23].

P0 temporal vein injections. P0 HSA_{LR} mouse pups were placed on wet ice for 30–60 s for anaesthesia. Using a dissection microscope, the superficial temporal vein was identified, and the tip of a 36 gauge needle (NANOFIL; World Precision Instruments) was inserted into the temporal vein. AAV9 (40 µl, 10^{11} vg) was then injected using a 50 µl Hamilton syringe and a digital infusion pump (Microinjector MINJ-PD; Tritech Research) at a rate of 1 µl s^{-1}. After vector delivery, the needle remained in the vein for 15 s to prevent backflow of the vector. After removing the needle, gentle pressure was applied using a cotton swab to stop the bleeding. The pups were rewarmed in the investigator's gloved hands to provide appropriate warmth for 2–3 min. When the pups were fully recovered, they were returned to the cage.

TA injections. Mice were anaesthetized with inhalational anaesthesia using 3% isoflurane for induction and 1.5% isoflurane for maintenance. For TA injections, AAV9 containing either RCas9-CTG or RCas9-NT was thawed on ice, diluted in sterile phosphate-buffered saline (PBS) and injected (30 µl) into the TA muscle (shaved and tendons exposed) of FVB or HSA_{LR} anaesthetized mice (aged 6–8 weeks) using a 29 gauge needle.

Immunosuppression. Immunosuppression was performed with tacrolimus (0.5 mg kg^{-1} d^{-1}), delivered as a single subcutaneous injection of a 12 d releasable microsphere formulation as described previously[79]. CTLA4-Ig was delivered by an intraperitoneal injection at a dose of 200 µg per animal[56]. The immunosuppression was administered 2 d before AAV9 administration.

RNA-FISH analysis. TA cryosections (8–10 µM) were fixed for 10 min with 4% PFA in 1× PBS. The sections were washed with 1× PBS three times and permeabilized in the 2% acetone (in water) at room temperature for 5 min. Next, acetone was removed, and sections were rehydrated for 10 min with wash buffer containing 40% formamide and 2× SSC buffer. Sections were then incubated with prehybridization buffer (10% dextran sulfate, 2 mM ribonucleoside vanadyl complex, 2× SSC pH 5, 50% fresh and deionized RNase-free formamide, 200 µg ml^{-1} bovine serum albumin, 1 mg ml^{-1} yeast tRNA, diethylpyrocarbonate-treated water to attain the final target volume) for 15 min at 37 °C in a hybridization oven. CAG10 probe was denatured at 98 °C for 10 min, and 500 pg µl^{-1} (final concentration) of the probe was added to cold prehybridization buffer and immediately added to the sections. The sections were hybridized for 2 h at 37 °C in a hybridization oven. The sections were next washed three times for 30 min each with wash buffer. Sections were then washed once with PBS and slides were mounted with 4,6-diamidino-2-phenylindole (DAPI) containing-mounting medium (ProLong Diamond Antifade Mountant with DAPI). Image quantification (Fig. 1c and Supplementary Fig. 1b) was conducted by counting the number of RNA foci in the presence of non-targeting or RCas9-CTG.

RNA-seq library preparation and data processing. Library preparation and sequencing was performed as described previously[80]. Total RNA was isolated using TRIzol reagent (Life technologies) and treated with Turbo DNase (Life Technologies). Libraries were prepared using the Illumina TruSeq polyA+ mRNA sample preparation reagents according to the manufacturer's protocol. All of the samples were sequenced using the Illumina HiSeq 4000 platform. Demultiplexed FASTQ files were checked for quality and aligned to the mm10 mouse genome platform. Cluster v.3.0 and Java Treeview were used in combination to perform and visualize results the hierarchical gene expression clustering results. For splicing analysis, we used the Olego and Quantas software suite as previously described[80,81]. RNA-seq data processing involved alignment with the Olego de novo splice junction aligner and were quantified using Quantas. Quantas calculates exon inclusion indices (splicing index equivalent to PSI values) and differential splicing measures between two groups (dI values). Fisher's exact test in Quantas was used to call FDR-adjusted *P* values. As thresholds, we used FDR-adjusted $P<0.05$ and $dI>|0.15|$ as statistically significant alternative splicing events.

Statistics and power analysis. Using an a priori calculation for a *t*-test difference between two independent means based on a normally distributed population with equal variance (a significance level of 0.05, an effect size of 2 and a power of 0.90), 6 animals per group would be required to determine whether there is a significant difference between groups treated with RCas9-CTG or RCas9-NT at a single dose. On the basis of our experience, we estimated a survival rate of >99% of treated HSA_{LR} mice to the end of the testing age. As DM1 occurs with equal frequency in both males and females, equal numbers of both male and female mice were used whenever possible. Two-tailed Student's *t*-tests (Microsoft Excel) with unequal variances were performed to test the null hypothesis that the treated groups were not different in a pairwise comparison when the distribution of sample populations was expected to be normal. Mann–Whitney *U*-tests and *Z*-score analysis were used to analyse between treated groups in a pairwise manner when the assumption of

normality was in question. For alternative-splicing analysis using RNA-seq data, Fisher's exact test was performed using the Quantas software package (https://zhanglab.c2b2.columbia.edu/index.php/Quantas_Documentation), measuring the total number of splice-junction reads supporting each isoform to calculate the exon inclusion level and the change between the two groups.

H&E and immunostaining. Frozen sections (thickness, 8–10 µm) of TA muscle were either prepared for routine H&E staining or immunostained using antibodies against the ClC-1/CLCN1 C terminus (CLC12a from Alpha Diagnostic) or the MBNL1 C-terminal peptide (rabbit polyclonal antibody A2764 from the University of Florida) as described previously[23]. For MBNL1, sections were fixed in 4% PFA for 10 min at room temperature and permeabilized with 2% acetone (in water) in PBS for 5 min. Sections were left unfixed for CLCN1 and permeabilized in 2% acetone (in water) in PBS for 5 min. Primary antibody concentrations were 1:1,000 for MBNL1 and 1:100 for CLCN1. The secondary antibodies used were goat anti-rabbit Alexa Fluor 488 and 546 (Thermo Fisher Scientific) at 1:500 dilution.

CD3 immunohistochemistry. Sections were cut at 4 µm, dewaxed and rehydrated in distilled water before antigen retrieval (AR). This was achieved by placing 200 ml of AR reagent into a staining dish and heating for 10 min. Once the AR reagent cooled, the slides were removed and placed into an autostainer (Thermo Fisher Scientific). Endogenous peroxidase and non-specific proteins were blocked for 10 mins using 3% H_2O_2 and 3% normal goat serum, respectively, followed by buffer washes. CD3-specific primary antibodies (Abcam, ab5690) were added onto the section and incubated for 1 h and then washed three times with PBS. The primary antibodies were detected using goat anti-rabbit HRP-conjugated antibodies, and visualized by incubating with DAB substrate and counterstaining with haematoxylin. The slides were then dehydrated in ethanol and mounted in xylene before microscopy examination.

RNA splicing RT–PCR. RNAs were isolated from TA muscle using TriReagent (Sigma-Aldrich) according to the manufacturer's protocol, and cDNAs were generated and PCR-amplified using GoTaq (Promega) Taq polymerase using specific primers (Supplementary Table 5). PCR products were resolved on either 2% agarose-TBE gels or with the Agilent 2200 Tapestation. The gels were visualized using an Amersham Imager 680.

Electromyography. Mice were anaesthetized by inhalational anaesthesia using 3% isoflurane for induction and 1.5% isoflurane for maintenance. Electromyography was performed using TECA elite 30 gauge concentric needle electrodes on a Teca Synergy system (MFI medical) as described by Chamberlain et al.[82]. The needle electrode was inserted at least ten times for each muscle analysed (TA). The frequency of insertions yielding a myotonic discharge was recorded for each mouse ($n=6$ for each control and RCas9-CTG groups). The individual performing electromyography analysis was blinded to mouse genotypes.

Animal work. Animal work was carried out at the University of Florida (supported by NIH grant NS103172) and Explora Biolabs (supported by Locana) according to the respective IACUC protocols.

Reporting Summary. Further information on research design is available in the Nature Research Reporting Summary linked to this article.

Data availability

The main data supporting the results in this study are available within the paper and its Supplementary Information. Intramuscular RCas9 injection NGS data are available at the GEO repository (GSE152033) and can also be viewed using the UCSC genome browser (https://genome.ucsc.edu/s/ranjan99/RCas9_HSA_IM). The raw and analysed datasets generated during the study are available for research purposes from the corresponding author on reasonable request.

Received: 13 May 2019; Accepted: 10 August 2020;
Published online: 14 September 2020

References

1. Iyer, R. R., Pluciennik, A., Napierala, M. & Wells, R. D. DNA triplet repeat expansion and mismatch repair. *Annu. Rev. Biochem.* **84**, 199–226 (2015).
2. Dion, V. Tissue specificity in DNA repair: lessons from trinucleotide repeat instability. *Trends Genet.* **30**, 220–229 (2014).
3. Lopez Castel, A., Cleary, J. D. & Pearson, C. E. Repeat instability as the basis for human diseases and as a potential target for therapy. *Nat. Rev. Mol. Cell Biol.* **11**, 165–170 (2010).
4. McGinty, R. J. & Mirkin, S. M. *Cis*- and *trans*-modifiers of repeat expansions: blending model systems with human genetics. *Trends Genet.* **34**, 448–465 (2018).
5. Pearson, C. E. Slipping while sleeping? Trinucleotide repeat expansions in germ cells. *Trends Mol. Med.* **9**, 490–495 (2003).
6. Schmidt, M. H. M. & Pearson, C. E. Disease-associated repeat instability and mismatch repair. *DNA Repair* **38**, 117–126 (2016).
7. Cinesi, C., Aeschbach, L., Yang, B. & Dion, V. Contracting CAG/CTG repeats using the CRISPR–Cas9 nickase. *Nat. Commun.* **7**, 13272 (2016).
8. Dastidar, S. et al. Efficient CRISPR/Cas9-mediated editing of trinucleotide repeat expansion in myotonic dystrophy patient-derived iPS and myogenic cells. *Nucleic Acids Res.* **46**, 8275–8298 (2018).
9. Lo Scrudato, M. et al. Genome editing of expanded CTG repeats within the human *DMPK* gene reduces nuclear RNA foci in the muscle of DM1 mice. *Mol. Ther.* **27**, 1372–1388 (2019).
10. Provenzano, C. et al. CRISPR/Cas9-mediated deletion of CTG expansions recovers normal phenotype in myogenic cells derived from myotonic dystrophy 1 patients. *Mol. Ther. Nucleic Acids* **9**, 337–348 (2017).
11. van Agtmaal, E. L. et al. CRISPR/Cas9-induced $(CTGCAG)_n$ repeat instability in the myotonic dystrophy type 1 locus: implications for therapeutic genome editing. *Mol. Ther.* **25**, 24–43 (2017).
12. La Spada, A. R., Wilson, E. M., Lubahn, D. B., Harding, A. E. & Fischbeck, K. H. Androgen receptor gene mutations in X-linked spinal and bulbar muscular atrophy. *Nature* **352**, 77–79 (1991).
13. La Spada, A. R. & Taylor, J. P. Repeat expansion disease: progress and puzzles in disease pathogenesis. *Nat. Rev. Genet.* **11**, 247–258 (2010).
14. O'Rourke, J. R. & Swanson, M. S. Mechanisms of RNA-mediated disease. *J. Biol. Chem.* **284**, 7419–7423 (2009).
15. Batra, R., Manchanda, M. & Swanson, M. S. Global insights into alternative polyadenylation regulation. *RNA Biol.* **12**, 597–602 (2015).
16. Renton, A. E. et al. A hexanucleotide repeat expansion in C9ORF72 is the cause of chromosome 9p21-linked ALS-FTD. *Neuron* **72**, 257–268 (2011).
17. DeJesus-Hernandez, M. et al. Expanded GGGGCC hexanucleotide repeat in noncoding region of C9ORF72 causes chromosome 9p-linked FTD and ALS. *Neuron* **72**, 245–256 (2011).
18. Wilburn, B. et al. An antisense CAG repeat transcript at *JPH3* locus mediates expanded polyglutamine protein toxicity in Huntington's disease-like 2 mice. *Neuron* **70**, 427–440 (2011).
19. Du, J. et al. RNA toxicity and missplicing in the common eye disease Fuchs endothelial corneal dystrophy. *J. Biol. Chem.* **290**, 5979–5990 (2015).
20. The Huntington's Disease Collaborative Research Group. A novel gene containing a trinucleotide repeat that is expanded and unstable on Huntington's disease chromosomes. *Cell* **72**, 971–983 (1993).
21. Miller, J. W. et al. Recruitment of human muscleblind proteins to $(CUG)_n$ expansions associated with myotonic dystrophy. *EMBO J.* **19**, 4439–4448 (2000).
22. Shin, J., Charizanis, K. & Swanson, M. S. Pathogenic RNAs in microsatellite expansion disease. *Neurosci. Lett.* **466**, 99–102 (2009).
23. Kanadia, R. N. et al. Reversal of RNA missplicing and myotonia after muscleblind overexpression in a mouse poly(CUG) model for myotonic dystrophy. *Proc. Natl Acad. Sci. USA* **103**, 11748–11753 (2006).
24. Batra, R. et al. Loss of MBNL leads to disruption of developmentally regulated alternative polyadenylation in RNA-mediated disease. *Mol. Cell* **56**, 311–322 (2014).
25. Wheeler, T. M., Lueck, J. D., Swanson, M. S., Dirksen, R. T. & Thornton, C. A. Correction of ClC-1 splicing eliminates chloride channelopathy and myotonia in mouse models of myotonic dystrophy. *J. Clin. Invest.* **117**, 3952–3957 (2007).
26. Du, H. et al. Aberrant alternative splicing and extracellular matrix gene expression in mouse models of myotonic dystrophy. *Nat. Struct. Mol. Biol.* **17**, 187–193 (2010).
27. Kumar, A., Agarwal, S., Agarwal, D. & Phadke, S. R. Myotonic dystrophy type 1 (DM1): a triplet repeat expansion disorder. *Gene* **522**, 226–230 (2013).
28. Johnson, N. et al. Genetic prevalence of myotonic dystrophy type 1. *Neurology* **92**, S23.003 (2019).
29. Wang, Y. et al. Therapeutic genome editing for myotonic dystrophy type 1 using CRISPR/Cas9. *Mol. Ther.* **26**, 2617–2630 (2018).
30. Krishnan, J., Athar, F., Rani, T. S. & Mishra, R. K. Simple sequence repeats showing 'length preference' have regulatory functions in humans. *Gene* **628**, 156–161 (2017).
31. Wheeler, T. M. et al. Reversal of RNA dominance by displacement of protein sequestered on triplet repeat RNA. *Science* **325**, 336–339 (2009).
32. Pinto, B. S. et al. Impeding transcription of expanded microsatellite repeats by deactivated Cas9. *Mol. Cell* **68**, 479–490 (2017).
33. Bisset, D. R. et al. Therapeutic impact of systemic AAV-mediated RNA interference in a mouse model of myotonic dystrophy. *Hum. Mol. Genet.* **24**, 4971–4983 (2015).
34. Rzuczek, S. G. et al. Precise small-molecule recognition of a toxic CUG RNA repeat expansion. *Nat. Chem. Biol.* **13**, 188–193 (2017).
35. Grimm, D. et al. Argonaute proteins are key determinants of RNAi efficacy, toxicity, and persistence in the adult mouse liver. *J. Clin. Invest.* **120**, 3106–3119 (2010).
36. Janas, M. M. et al. Selection of GalNAc-conjugated siRNAs with limited off-target-driven rat hepatotoxicity. *Nat. Commun.* **9**, 723 (2018).

37. Batra, R. et al. Elimination of toxic microsatellite repeat expansion RNA by RNA-targeting Cas9. *Cell* **170**, 899–912 (2017).
38. Lagrue, E. et al. A large multicenter study of pediatric myotonic dystrophy type 1 for evidence-based management. *Neurology* **92**, e852–e865 (2019).
39. Mankodi, A. et al. Myotonic dystrophy in transgenic mice expressing an expanded CUG repeat. *Science* **289**, 1769–1773 (2000).
40. Lee, J. E., Bennett, C. F. & Cooper, T. A. RNase H-mediated degradation of toxic RNA in myotonic dystrophy type 1. *Proc. Natl Acad. Sci. USA* **109**, 4221–4226 (2012).
41. Wheeler, T. M. et al. Targeting nuclear RNA for in vivo correction of myotonic dystrophy. *Nature* **488**, 111–115 (2012).
42. Chen, B. et al. Dynamic imaging of genomic loci in living human cells by an optimized CRISPR/Cas system. *Cell* **155**, 1479–1491 (2013).
43. Bengtsson, N. E. et al. Muscle-specific CRISPR/Cas9 dystrophin gene editing ameliorates pathophysiology in a mouse model for Duchenne muscular dystrophy. *Nat. Commun.* **8**, 14454 (2017).
44. Lin, X. et al. Failure of MBNL1-dependent post-natal splicing transitions in myotonic dystrophy. *Hum. Mol. Genet.* **15**, 2087–2097 (2006).
45. Kalsotra, A. et al. A postnatal switch of CELF and MBNL proteins reprograms alternative splicing in the developing heart. *Proc. Natl Acad. Sci. USA* **105**, 20333–20338 (2008).
46. Charizanis, K. et al. Muscleblind-like 2-mediated alternative splicing in the developing brain and dysregulation in myotonic dystrophy. *Neuron* **75**, 437–450 (2012).
47. Poulos, M. G. et al. Progressive impairment of muscle regeneration in muscleblind-like 3 isoform knockout mice. *Hum. Mol. Genet.* **22**, 3547–3558 (2013).
48. Wagner, S. D. et al. Dose-dependent regulation of alternative splicing by MBNL proteins reveals biomarkers for myotonic dystrophy. *PLoS Genet.* **12**, e1006316 (2016).
49. Nakamori, M. et al. Splicing biomarkers of disease severity in myotonic dystrophy. *Ann. Neurol.* **74**, 862–872 (2013).
50. Sebastian, S. et al. Tissue-specific splicing of a ubiquitously expressed transcription factor is essential for muscle differentiation. *Genes Dev.* **27**, 1247–1259 (2013).
51. Thomas, J. D., Oliveira, R., Sznajder, L. J. & Swanson, M. S. Myotonic dystrophy and developmental regulation of RNA processing. *Compr. Physiol.* **8**, 509–553 (2018).
52. Huang, D., Sherman, B. T. & Lempicki, R. A. Systematic and integrative analysis of large gene lists using DAVID bioinformatics resources. *Nat. Protoc.* **4**, 44–57 (2009).
53. Amack, J. D. & Mahadevan, M. S. Myogenic defects in myotonic dystrophy. *Dev. Biol.* **265**, 294–301 (2004).
54. Konermann, S. et al. Transcriptome engineering with RNA-targeting type VI-D CRISPR effectors. *Cell* **173**, 665–676 (2018).
55. Yan, W. X. et al. Cas13d is a compact RNA-targeting type VI CRISPR effector positively modulated by a WYL-domain-containing accessory protein. *Mol. Cell* **70**, 327–339 (2018).
56. Guibinga, G. H. et al. Combinatorial blockade of calcineurin and CD28 signaling facilitates primary and secondary therapeutic gene transfer by adenovirus vectors in dystrophic (*mdx*) mouse muscles. *J. Virol.* **72**, 4601–4609 (1998).
57. Wang, Z. et al. Immunity to adeno-associated virus-mediated gene transfer in a random-bred canine model of Duchenne muscular dystrophy. *Hum. Gene Ther.* **18**, 18–26 (2007).
58. Zhou, J., Liu, B., Liang, C., Li, Y. & Song, Y. H. Cytokine signaling in skeletal muscle wasting. *Trends Endocrinol. Metab.* **27**, 335–347 (2016).
59. Mammarella, A. et al. Tumor necrosis factor-alpha and myocardial function in patients with myotonic dystrophy type 1. *J. Neurol. Sci.* **201**, 59–64 (2002).
60. Nakamori, M. et al. Aberrant myokine signaling in congenital myotonic dystrophy. *Cell Rep.* **21**, 1240–1252 (2017).
61. Zhang, L., Lee, J. E., Wilusz, J. & Wilusz, C. J. The RNA-binding protein CUGBP1 regulates stability of tumor necrosis factor mRNA in muscle cells: implications for myotonic dystrophy. *J. Biol. Chem.* **283**, 22457–22463 (2008).
62. Ward, A. J., Rimer, M., Killian, J. M., Dowling, J. J. & Cooper, T. A. CUGBP1 overexpression in mouse skeletal muscle reproduces features of myotonic dystrophy type 1. *Hum. Mol. Genet.* **19**, 3614–3622 (2010).
63. Sznajder, L. J. et al. Loss of MBNL1 induces RNA misprocessing in the thymus and peripheral blood. *Nat. Commun.* **11**, 2022 (2020).
64. Yang, L. et al. A myocardium tropic adeno-associated virus (AAV) evolved by DNA shuffling and in vivo selection. *Proc. Natl Acad. Sci. USA* **106**, 3946–3951 (2009).
65. Lai, Y. et al. Efficient in vivo gene expression by trans-splicing adeno-associated viral vectors. *Nat. Biotechnol.* **23**, 1435–1439 (2005).
66. Trapani, I. Adeno-associated viral vectors as a tool for large gene delivery to the retina. *Genes* **10**, 287 (2019).
67. Choudhury, R., Tsai, Y. S., Dominguez, D., Wang, Y. & Wang, Z. Engineering RNA endonucleases with customized sequence specificities. *Nat. Commun.* **3**, 1147 (2012).
68. Hagedorn, P. H. et al. Identifying and avoiding off-target effects of RNase H-dependent antisense oligonucleotides in mice. *Nucleic Acids Res.* **46**, 5366–5380 (2018).
69. Nelson, C. E. et al. Long-term evaluation of AAV-CRISPR genome editing for Duchenne muscular dystrophy. *Nat. Med.* **25**, 427–432 (2019).
70. Ferdosi, S. R. et al. Multifunctional CRISPR–Cas9 with engineered immunosilenced human T cell epitopes. *Nat. Commun.* **10**, 1842 (2019).
71. Hinderer, C. et al. Neonatal systemic AAV induces tolerance to CNS gene therapy in MPS I dogs and nonhuman primates. *Mol. Ther.* **23**, 1298–1307 (2015).
72. Cooper, M. et al. Improved induction of immune tolerance to factor IX by hepatic AAV-8 gene transfer. *Hum. Gene Ther.* **20**, 767–776 (2009).
73. Doerfler, P. A. et al. Copackaged AAV9 vectors promote simultaneous immune tolerance and phenotypic correction of Pompe disease. *Hum. Gene Ther.* **27**, 43–59 (2016).
74. Puzzo, F. et al. Rescue of Pompe disease in mice by AAV-mediated liver delivery of secretable acid α-glucosidase. *Sci. Transl. Med.* **9**, eaam6375 (2017).
75. Nelles, D. A. et al. Programmable RNA tracking in live cells with CRISPR/Cas9. *Cell* **165**, 488–496 (2016).
76. O'Connell, M. R. et al. Programmable RNA recognition and cleavage by CRISPR/Cas9. *Nature* **516**, 263–266 (2014).
77. Cox, D. B. T. et al. RNA editing with CRISPR–Cas13. *Science* **358**, 1019–1027 (2017).
78. Bravo-Hernandez, M. Spinal subpial delivery of AAV9 enables widespread gene silencing and blocks motoneuron degeneration in ALS. *Nat. Med.* **26**, 118–130 (2020).
79. Bravo-Hernandez, M. et al. Spinal subpial delivery of AAV9 enables widespread gene silencing and blocks motoneuron degeneration in ALS. *Nat. Med.* **26**, 118–130 (2020).
80. Batra, R. et al. RNA-binding protein CPEB1 remodels host and viral RNA landscapes. *Nat. Struct. Mol. Biol.* **23**, 1101–1110 (2016).
81. Wu, J., Anczukow, O., Krainer, A. R., Zhang, M. Q. & Zhang, C. OLego: fast and sensitive mapping of spliced mRNA-seq reads using small seeds. *Nucleic Acids Res.* **41**, 5149–5163 (2013).
82. Chamberlain, C. M. & Ranum, L. P. W. Mouse model of muscleblind-like 1 overexpression: skeletal muscle effects and therapeutic promise. *Hum. Mol. Genet.* **21**, 4645–4654 (2012).

Acknowledgements

This work was partially supported by the NIH (grant no. NS103172) to G.W.Y. and M.S.S. This work is also partially supported by the Muscular Dystrophy Association MVP (grant no. 575855) to R.B. and Locanabio.

Author contributions

G.W.Y., R.B., D.A.N. and M.S.S. conceptualized and designed the study and wrote the paper. R.B., D.A.N., F.K. and H.L.G. performed tissue sectioning, staining and histopathology. R.B., D.M.R., S.M.B. and H.L.G. performed RNA extractions and qPCR. M.S.S. provided the HSA_{LR} mouse colony. R.B., J.D.T., C.A.N. and Ł.J.S. maintained the HSA_{LR} colony, performed adult injections and collected tissues. T.T. and M.M. performed P0 neonatal injections. S.A. and R.B. generated next-generation sequencing (NGS) libraries. R.B., P.L., F.K. and G.W.Y. performed NGS data analysis. A.M. packaged AAV and performed quality control of the virus. R.B., O.P. and M.M. performed electrophysiology. R.B. performed functional assays. R.B., D.A.N. and G.W.Y. analysed all data. G.W.Y. supervised the study.

Competing interests

G.W.Y. is a cofounder, member of the board of directors, equity holder and paid consultant of Locanabio. D.A.N. is a cofounder and an equity holder of Locanabio. R.B. is an equity holder and employee of Locanabio. M.S.S. is an equity holder of Locanabio and a Scientific Advisory Board member of Skyhawk Therapeutics. The terms of this arrangement have been reviewed and approved by the University of California San Diego and the University of Florida, Gainesville in accordance with their conflict of interest policies. The other authors declare no other competing interests.

Additional information

Supplementary information Supplementary information is available for this paper at https://doi.org/10.1038/s41551-020-00607-7.

Correspondence and requests for materials should be addressed to G.W.Y.

Reprints and permissions information is available at www.nature.com/reprints.

Publisher's note Springer Nature remains neutral with regard to jurisdictional claims in published maps and institutional affiliations.

nature research

Corresponding author(s): Gene Yeo

Last updated by author(s): Jun 28, 2020

Reporting Summary

Nature Research wishes to improve the reproducibility of the work that we publish. This form provides structure for consistency and transparency in reporting. For further information on Nature Research policies, see our Editorial Policies and the Editorial Policy Checklist.

Statistics

For all statistical analyses, confirm that the following items are present in the figure legend, table legend, main text, or Methods section.

n/a	Confirmed	
☐	☒	The exact sample size (*n*) for each experimental group/condition, given as a discrete number and unit of measurement
☐	☒	A statement on whether measurements were taken from distinct samples or whether the same sample was measured repeatedly
☐	☒	The statistical test(s) used AND whether they are one- or two-sided *Only common tests should be described solely by name; describe more complex techniques in the Methods section.*
☐	☒	A description of all covariates tested
☒	☐	A description of any assumptions or corrections, such as tests of normality and adjustment for multiple comparisons
☐	☒	A full description of the statistical parameters including central tendency (e.g. means) or other basic estimates (e.g. regression coefficient) AND variation (e.g. standard deviation) or associated estimates of uncertainty (e.g. confidence intervals)
☐	☒	For null hypothesis testing, the test statistic (e.g. *F*, *t*, *r*) with confidence intervals, effect sizes, degrees of freedom and *P* value noted *Give P values as exact values whenever suitable.*
☒	☐	For Bayesian analysis, information on the choice of priors and Markov chain Monte Carlo settings
☐	☒	For hierarchical and complex designs, identification of the appropriate level for tests and full reporting of outcomes
☐	☒	Estimates of effect sizes (e.g. Cohen's *d*, Pearson's *r*), indicating how they were calculated

Our web collection on statistics for biologists contains articles on many of the points above.

Software and code

Policy information about availability of computer code

Data collection	BioRad CFX software was used for qPCR. Agilent Tapestration controller was used for splicing gel analysis. Microsoft Excel was used for collection of the raw Ct files from qPCR data. Teca synergy EMG software (https://cdn.shopify.com/s/files/1/1046/1086/files/Viasys-TECA-Synergy-EMG-EP-Systems-User-Manual.pdf) was used to collect electromyography data.
Data analysis	Olego version v1.1.7 (https://zhanglab.c2b2.columbia.edu/index.php/OLego_Documentation) was used to align RNA-seq data and Quantas version v1.0.9 (https://zhanglab.c2b2.columbia.edu/index.php/Quantas_Documentation) was used for the analysis of gene expression and splicing. Cluster 3.0 (http://bonsai.hgc.jp/~mdehoon/software/cluster/software.htm) and Java Treeview 3.0 (http://jtreeview.sourceforge.net/) were used to generate and view hierarchical clustering. GPower software (free version) was used for power analysis. Box plots were generated using R in the webtool http://shiny.chemgrid.org/boxplotr/

For manuscripts utilizing custom algorithms or software that are central to the research but not yet described in published literature, software must be made available to editors and reviewers. We strongly encourage code deposition in a community repository (e.g. GitHub). See the Nature Research guidelines for submitting code & software for further information.

Data

Policy information about availability of data

All manuscripts must include a data availability statement. This statement should provide the following information, where applicable:

- Accession codes, unique identifiers, or web links for publicly available datasets
- A list of figures that have associated raw data
- A description of any restrictions on data availability

The main data supporting the results in this study are available within the paper and its Supplementary Information. Intramuscular RCas9 Injection NGS data are

available in the GEO repository (GSE152033) and can also be viewed via the UCSC genome browser at https://genome.ucsc.edu/s/ranjan99/RCas9_HSA_IM. The raw and analysed datasets generated during the study are available for research purposes from the corresponding authors on reasonable request.

Field-specific reporting

Please select the one below that is the best fit for your research. If you are not sure, read the appropriate sections before making your selection.

☒ Life sciences ☐ Behavioural & social sciences ☐ Ecological, evolutionary & environmental sciences

For a reference copy of the document with all sections, see nature.com/documents/nr-reporting-summary-flat.pdf

Life sciences study design

All studies must disclose on these points even when the disclosure is negative.

Sample size	The sample size required to achieve statistical power was determined by using standard power analysis via the GPower software. Using an a priori calculation for a t-test difference between two independent means based on a normally distributed population with equal variance (a significance level of 0.05, an effect size of 2 and a power of 0.90), the numbers of animals per group were calculated to determine significant differences between groups.
Data exclusions	Data were excluded from PO temporal vein injections if no transgene was expressed due to failure of the injection technique. No other data were excluded.
Replication	All data were replicated at least 3 times in different experiments.
Randomization	Mice were used in a random manner after genotyping at a specific age. All samples were processed randomly, sequenced, and analysed in a blind manner.
Blinding	All physiological and imaging analyses of mouse samples were done in a blinded manner.

Reporting for specific materials, systems and methods

We require information from authors about some types of materials, experimental systems and methods used in many studies. Here, indicate whether each material, system or method listed is relevant to your study. If you are not sure if a list item applies to your research, read the appropriate section before selecting a response.

Materials & experimental systems

n/a	Involved in the study
☐	☒ Antibodies
☒	☐ Eukaryotic cell lines
☒	☐ Palaeontology and archaeology
☐	☒ Animals and other organisms
☒	☐ Human research participants
☒	☐ Clinical data
☒	☐ Dual use research of concern

Methods

n/a	Involved in the study
☒	☐ ChIP-seq
☒	☐ Flow cytometry
☒	☐ MRI-based neuroimaging

Antibodies

Antibodies used	CD3 (Abcam # ab5690), ClC-1/CLCN1 C terminus (CLC12a from Alpha Diagnostic, San Antonio, TX)
Validation	CD3 antibody was validated using positive (spleen and lymph nodes) and negative (brain, no primary) controls. Clcn1 antibody was validated in mouse skeletal muscle (positive) and brain (negative) as controls. We also used no primary antibody controls for each staining.

Animals and other organisms

Policy information about studies involving animals; ARRIVE guidelines recommended for reporting animal research

Laboratory animals	FVB/NJ mice were ordered from the Jackson laboratory as WT controls. HSA-LR DMI mice on the FVB/NJ background were obtained from the Maurice Swanson Lab at University of Florida.
Wild animals	The study did not involve wild animals.
Field-collected samples	The study did not involve samples collected from the field.

Ethics oversight	UF IACUC, Explora Biolabs IACUC, 11175 Flintkote Ave, San Diego, CA 92121

Note that full information on the approval of the study protocol must also be provided in the manuscript.